https://doi.org/10.5194/esd-2024-16
Preprint. Discussion started: 15 July 2024
© Author(s) 2024. CC BY 4.0 License.

Earth System Dynamics
Discussions
Open Access
EGU

The European summer heatwave 2019 - a regional storyline perspective

Tatiana Klimiuk[1], Patrick Ludwig[1], Antonio Sanchez-Benitez[2], Helge F. Goessling[2], Peter Braesicke[3], and Joaquim G. Pinto[1]

[1]Institute of Meteorology and Climate Research - Tropospheric Research (IMKTRO), Karlsruhe Institute of Technology (KIT), Karlsruhe, Germany
[2]Alfred Wegener Institute Helmholtz-Center for Polar and Marine Research, Bremerhaven, Germany
[3]Institute of Meteorology and Climate Research - Atmospheric Trace Gases and Remote Sensing (IMKASF), Karlsruhe Institute of Technology (KIT), Karlsruhe, Germany

Correspondence: Tatiana Klimiuk (tatiana.klimiuk@kit.edu)

Abstract.

The number and intensity of heat waves have increased in the recent past, along with anthropogenic climate change. This poses challenges to many communities and raises the need to develop adaptation measures based on more accurate information regarding regional to local changes in temperature extremes and their impacts. While the general increase in global mean temperature is well established, current global climate projections show a large model spread regarding possible future circulation changes. To isolate the more certain thermodynamic response from the less certain dynamical response to anthropogenic climate change, we employ an event-based storyline approach comprising three steps. Firstly, the large-scale circulation in the free troposphere was spectrally nudged to the ERA5-reanalyses in the global coupled climate model AWI-CM-1.1-MR for a recent period (2017 - 2022), corresponding to +1.4 K global warming, and repeated under pre-industrial, +2 K, +3 K, and +4 K global warming climates. Secondly, the global storylines were dynamically downscaled with the regional ICON-CLM model to the Euro-CORDEX domain with a horizontal resolution of 12 km and, thirdly, to a Central-European (German) domain with a resolution of 3 km. The present study focuses on the 2019 summer heatwaves over Central Europe. We demonstrate the added value of downscaling global storyline integrations, indicating a significant improvement in present-day temperature patterns and a reduced error in daily 2m temperature relative to observations in Central Europe. The magnitude of the heatwave temperature response significantly exceeds the globally modelled background warming, with a distinct spatial and temporal variation in the regional increments. Our simulations indicate a general linear dependency of the 2m temperature response to the global warming level: the warming rates during the July 2019 heatwave ranged between factors of 2 and 3 in Central Europe, resulting in an anthropogenic warming of 8 to 12 °C in the +4 K climate. The spatial extent and the duration of the heat wave are also amplified in the warmer climates. With this three-step downscaling approach, we gain new insights into possible future changes in heat extremes in Central Europe, which apparently surpass global warming trends. Along with its scientific value, our method provides ways to facilitate communication of regional climate change information to the users.

https://doi.org/10.5194/esd-2024-16
Preprint. Discussion started: 15 July 2024
© Author(s) 2024. CC BY 4.0 License.

Earth System Dynamics Discussions
Open Access
EGU

1 Introduction

Heat waves are a major natural hazard worldwide, with the heat waves of 2003, 2010 and 2018 as prominent examples on the European continent (e.g., Fink et al., 2004; Barriopedro et al., 2011; Miralles et al., 2014; Spensberger et al., 2020). In the last two decades, Europe has witnessed an increase in the frequency, duration, and intensity of extreme heat events, which in turn is causing an increase in mortality rates, food and water insecurity, and long-term economic and cultural stress (Robine et al., 2008; García-Herrera et al., 2010; Perkins-Kirkpatrick and Lewis, 2020; Becker et al., 2022; Calvin et al., 2023; Knutzen et al., 2023). The general effects of climate change on heat wave characteristics have been demonstrated to be robust in recent studies that are usually aimed at estimating the attribution of human-induced greenhouse gas (GHG) forcing to the recent extreme events using observational records and at projecting future changes by means of climate modelling (e.g., Barriopedro et al., 2011, 2023). The traditional approaches that commonly imply multi-model averaging and probabilistic event attribution can provide an estimate of trends in frequency, intensity, and persistence of extreme events, but they lack clarity regarding the physical processes that are causing the changes (Shepherd, 2014).

One of the current scientific challenges is to disentangle the relative role of dynamical and thermodynamic contributions on future heat wave characteristics in attribution and projection studies (Shepherd, 2014, 2021; Sousa et al., 2020; Sánchez-Benítez et al., 2018). Thermodynamic effects, such as near-surface warming, moistening of the atmosphere, and effects from the partitioning of radiative and turbulent fluxes, show a relatively robust response to the anthropogenic GHG forcing in models and generally tend to have less internal variability (Deser et al., 2014; Wehrli et al., 2018). On the other hand, the dynamic effects that include changes in the position, strength and meandering of the jet stream, as well as changes in the occurrence of weather regimes and more local circulation patterns, are subject to larger uncertainties (Deser et al., 2014; Shepherd et al., 2018; Zappa, 2019). First, this is associated with the inherent model uncertainties and differences in parametrisations of unresolved processes in the models (Shepherd, 2014); second, the internal variability of the dynamical component of the atmosphere is responsible for a low signal-to-noise ratio in the studies aimed to quantify the regional response of extreme events to global warming (Deser et al., 2014; Shepherd, 2014, 2021; Wehrli et al., 2018; Barriopedro et al., 2023).

An alternative to circumvent the uncertainties associated with different atmospheric circulation changes under enhanced GHG forcing is to consider an event-based storyline approach, where the large-scale circulation in a global climate model (GCM) is forced to follow a reanalyses state by nudging the upper tropospheric winds, whereas the background climate corresponds to a specific warming level (Sánchez-Benítez et al., 2022; Athanase et al., 2024; van Garderen et al., 2021; Wehrli et al., 2020). Along with the uncertainty of changing dynamics, the internal variability is considerably reduced (Sánchez-Benítez et al., 2022), which improves the signal-to-noise ratio, giving us the opportunity to better quantify the actual event-specific thermodynamic response. Assuming the robustness of the quantification, we improve our understanding of the potential impacts of future extreme temperature events and communicate them to the public and authorities in a more understandable manner.

Nevertheless, GCMs have difficulty representing the regional climate mean and variability due to unresolved orography and shortcomings in model parameterizations associated with the coarse horizontal resolution (Giorgi and Gutowski Jr, 2015).

https://doi.org/10.5194/esd-2024-16
Preprint. Discussion started: 15 July 2024
© Author(s) 2024. CC BY 4.0 License.

Earth System Dynamics Discussions

For example, using global nudged storylines, Sánchez-Benítez et al. (2022) found a strong amplification for the July 2019 European heat wave under global warming; however, their global simulations underestimated the high-temperature extremes reached during the heatwave. An effective method to address the lack of precision in GCMs is to apply a regional climate model (RCM) to perform the dynamical downscaling of a GCM (Feser et al., 2011; Giorgi, 2019; Vautard et al., 2021). Commonly, the horizontal resolution of RCMs applied for the European domain is in the order of 10 - 12 km (e.g., Jacob et al., 2014; Giorgi and Gutowski Jr, 2015). Being computationally effective, this resolution allows for the production of large ensembles of simulations, which considerably improves the representation of relevant climatological variables compared to GCMs (Vautard et al., 2021). Nevertheless, convective processes can only be resolved by convective-permitting regional models (CPMs) operating at resolutions of less than 4 km (Prein et al., 2015; Giorgi, 2019; Hundhausen et al., 2023). Associated with explicitly resolved deep convection and better-captured processes in regions with complex topography, CPMs have been shown to add further value to RCM's representation of precipitation and near-surface temperature, especially in the regions with complex topography (Prein et al., 2015; Giorgi, 2019).

In this study, we go a step beyond the global storyline approach by providing a regional perspective of the heat wave that occurred in Europe during July 2019 and its unfolding in colder (pre-industrial) and warmer climates (see, e.g., Sánchez-Benítez et al., 2022; Sousa et al., 2020). With this aim, we dynamically downscale the global spectral nudged storylines for the summer 2019 heatwave for five different background climates ranging from pre-industrial to +4 K global warming for (Central) Europe. The approach utilises a global-to-regional (GCM-RCM-CPM) model chain comprising the global spectral nudged storyline simulations obtained from the global Alfred Wegener Institute coupled climate model AWI-CM-1.1-MR (hereafter referred to as AWI-CM1, Semmler et al., 2020) with the large-scale horizontal winds spectrally nudged to ERA5 (Hersbach et al., 2020), and the ICOsahedral Nonhydrostatic model in Climate Limited area Mode ICON-CLM (Pham et al., 2021) for the dynamical downscaling to 12 km horizontal grid spacing over Europe and subsequently to 3 km horizontal grid spacing over Central Europe. This approach permits the derivation of climate data at high resolution, thereby providing detailed information for attribution and impact studies.

We address the following research questions:

(1) How accurately can a regional event-based storyline simulation represent a recent event, and what is the added value compared to the global spectral nudged storyline simulation?

(2) What is the effect of climate change on the 2019 European heatwave based on the regional and convective-permitting ICON-CLM simulations?

(3) What is the local to regional extreme temperature scaling in response to global warming for an event like the 2019 heat wave, and how does it differ from the scaling of the global mean temperature?

The paper is structured as follows: Section 2 describes the global and regional model setups, as well as the datasets used for model validation. The main results are presented in Section 3, with the first research question addressed in Section 3.1 and the regional storylines analysed in Sections 3.2 and 3.3. Section 4 summarises and discusses the results, formulates the main conclusions for each research question, and provides future research ideas.

https://doi.org/10.5194/esd-2024-16
Preprint. Discussion started: 15 July 2024
© Author(s) 2024. CC BY 4.0 License.

Earth System Dynamics Discussions
Open Access
EGU

2 Data and methods

2.1 Global Spectrally Nudged Storylines

The global spectral nudged simulations are based on the global coupled climate model AWI-CM1 (Semmler et al., 2020). This model has contributed to phase 6 of the Coupled Model Intercomparison Project (CMIP6, Eyring et al., 2016). It consists of the atmospheric model ECHAM6.3.04p1 from MPI-M (Stevens et al., 2013) coupled to the Finite Element Sea Ice–Ocean Model (FESOM) v.1.4 for the ocean component (Wang et al., 2014). The atmospheric component is run at a T127L95 spectral resolution, which corresponds to a horizontal resolution of about 100 km in the tropics and 95 vertical levels going up to ∼0.01 hPa. The ocean model FESOM uses an unstructured mesh that allows for fine resolution in energetically active areas such as the Gulf Stream (Sidorenko et al., 2015; Sein et al., 2017). Consequently, the horizontal resolution of the ocean ranges from 80 km in the subtropical Pacific to 8-10 km in the North Sea or 8-20 km in the Arctic (see Fig. 1 in Semmler et al., 2020).

In AWI-CM1, the large-scale atmospheric circulation is constrained by nudging the model's vorticity and divergence (representing the large-scale horizontal winds) to ERA5 reanalysis data (Hersbach et al., 2020) with an e-folding time of 24 h and a spectral truncation of 20 on zonal wavenumbers. Nudging is applied only to vertical levels between 700 and 100 hPa. This configuration has been shown to optimally constrain large-scale events such as heatwaves (Sánchez-Benítez et al., 2022), warm and moist intrusions in the Arctic (Pithan et al., 2023) or Marine heatwaves (Athanase et al., 2024), while preserving some freedom in the boundary layer and at small spatiotemporal timescales.

A series of nudged storyline simulations were conducted using ESM Tools (Barbi et al., 2021) for a range of climate states based on the configuration described above. Specifically, nudging experiments were branched off the historical CMIP6 runs (Semmler et al., 2020) on 1st of January 1851 to produce pre-industrial climate conditions. Meanwhile, present-day (+1.4 K) and +2 K, +3 K, +4 K climates relative to pre-industrial were made by spawning the shared socioeconomic pathway scenario ssp370 CMIP6 experiments (Semmler et al., 2019) on 1st of January 2017, 2038, 2065, and 2093, respectively. These years were selected according to when the global warming levels were reached. All storylines comprise five ensemble members, each spawned from the five respective CMIP6 simulations and thus started from slightly different initial conditions. Each storyline is simulated continuously from the 1st of January of the year corresponding to 2017 in the present-day climate (dynamical year 2017) to the 31st of September of the dynamical year 2022.

2.2 Dynamical downscaling with ICON-CLM

Next, the data from the global spectral nudged storylines described in Section 2.1 were used as initial and boundary conditions to drive the ICON model Version 2.6.5.1 (Zängl et al., 2015), in a regional climate configuration known as ICON-CLM (Pham et al., 2021). We use the runtime environment "Starter Package for ICON-CLM Experiments" SPICE v.2.0 (Rockel and Geyer, 2022) to conduct all the simulations. For each storyline, we simulate the full period 2017-2022 described in Section 2.1. Given that the spread of the ensemble during heatwaves is sufficiently small, as shown in Sánchez-Benítez et al. (2022), we utilise one ensemble member of the AWI-CM1 simulations in this study. The downscaling is performed on the Euro-CORDEX domain (Jacob et al., 2014) at R12B5 resolution corresponding to a horizontal grid spacing of 0.11° or 12 km, hereafter referred to as

https://doi.org/10.5194/esd-2024-16
Preprint. Discussion started: 15 July 2024
© Author(s) 2024. CC BY 4.0 License.

Earth System Dynamics
Discussions
Open Access
EGU

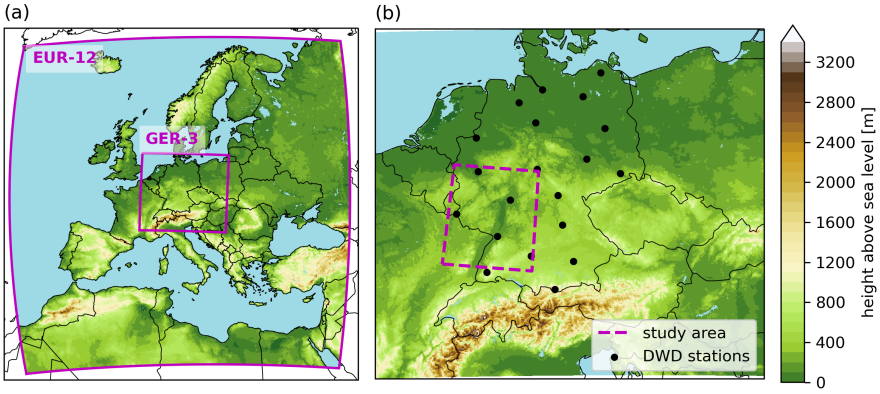

Figure 1. (a) EUR-12 and GER-3 domains used for downscaling the global AWI-CM1 storylines with ICON-CLM. (b) GER-3 domain with the locations of DWD (German Weather Service) observation stations and the area used for spatial averaging (48° N - 51° N, 6° E - 10° E). Shading corresponds to the respective orography used in the simulations.

EUR-12 (see Fig. 1a). Subsequently, we run a nested ICON-CLM simulation at R13B7 resolution, corresponding to 0.0275° or 3 km horizontal grid spacing for the extended German domain GER-3, including the peripheral hydrological catchment areas (see Fig. 1b).

In the upper boundary, grid point nudging was applied in the ICON-CLM simulations to maintain proximity to the present-time circulation represented by the global spectral nudged AWI-CM1 runs. In ICON, this nudging is implemented as an additional forcing term that is being added to the prognostic equations at each fast physics time step (Prill et al., 2023):

$$\psi(t) = \psi^*(t) + \alpha_{nudge} N_{ds} [\psi_{bc}(t) - \psi^*(t)] \tag{1}$$

Where $\psi_{bc}(t)$ is the value of the prognostic variable ψ at the time t taken from the driving model, ψ^* is the value of the variable ψ before the nuging, while α_{nudge} refers to the nudging strength, and N_{ds} is the number of dynamics substeps per fast physics step (Prill et al., 2023). Upper boundary nudging is applied in a sponge layer of the chosen thickness, where the nudging strength increases quadratically with height, starting with zero at the nudging start height z_{start} and reaching the maximum nudging coefficient B_0 at the model's top height:

$$\alpha_{nudge} = B_0 \left(\frac{z - z_{start}}{z_{top} - z_{start}} \right) \tag{2}$$

The nudging coefficient for the thermodynamic prognostic variables θ_v, ρ, and q_v was set to zero to prevent overfitting and, even more importantly in the context here, to allow for the free development of thermodynamics. Thus, upper boundary nudging was applied only to the horizontal velocity vn. We kept the maximum coefficient B_0 at its default value of 0.04. The nudging start height z_{start} in the EUR-12 domain was set to 5000 m, while for the GER-3, it was left at 10500 m to prevent interaction with deep convection. Further information can be found in Prill et al. (2023).

https://doi.org/10.5194/esd-2024-16
Preprint. Discussion started: 15 July 2024
© Author(s) 2024. CC BY 4.0 License.

Earth System Dynamics Discussions

Soil temperature and soil moisture data from ERA5 were used for soil initialisation in all storylines. For the present-time experiment, the initial simulation year (2017) was considered for spin-up. In the storyline simulations, an additional year was required for the soil to adapt to the warmer climate. Therefore, we ran the dynamical year 2017 twice. Eventually, the temperature of the lowermost soil level (T_CL) was adjusted to reflect the respective global warming level for each storyline. This adjustment was made based on the climatology of the 2m temperature of the respective AWI-CM1 storyline simulation.

2.3 Validation approach

We compare the obtained daily 2m temperature fields to the ERA5 reanalyses (Hersbach et al., 2020), as well as to the daily gridded land-only observational dataset over Europe E-OBS v.28 (see e.g., Cornes et al., 2018). The differences with respect to E-OBS are considered significant if their magnitude is larger than half of the ensemble spread of the observational dataset. To evaluate the simulations on the station level, we use 20 stations of the German National Weather Service (DWD, 2023; Kaspar et al., 2013, see the full list in Table S1).

The root mean square difference (RMSD) to observational datasets (DWD and E-OBS) and its change between simulations of different resolutions (ΔRMSD) is chosen as a metric to quantify the added value. The significance of ΔRMSD between ICON EUR-12 and GER-3 is computed with the paired difference test (Rubin, 1973).

3 Results

3.1 Validation of the present-day storylines

The results of the ICON regional model simulations are evaluated by comparing the model's output with observational E-OBS and ERA5-reanalysis data. The comparison of the 2m temperature and 500-hPa geopotential height fields for the heatwave peaks of June and July 2019 shows a good agreement between the ICON EUR-12 simulations (Figure 2c,f) and ERA5 reanalyses (Fig. 2a,d). Furthermore, the ICON simulation shows a clear improvement in the representation of daily 2m temperature compared to the global AWI-CM1 simulation (Fig. 2b,e). The comparison of the daily temperature fields to E-OBS yielded similar results (see Fig. S1)

In Fig. 3, the time series of daily maximum, mean, and minimum 2m temperatures are compared to E-OBS over the longitude/latitude area 48° N - 51° N, 6° E - 10° E, to investigate the underestimation of maximum temperature during the exceptionally hot periods in June and July 2019 mentioned in Sánchez-Benítez et al. (2022). The ICON simulations show an improvement both for the daily maximum and minimum temperatures in July in this area. This indicates a more accurate representation of the diurnal temperature range in the regional ICON simulations.

In order to assess the added value of the ICON simulations, we calculated the root mean square difference (RMSD) in June - August of the simulated 2m temperature with respect to DWD observations (DWD, 2023) using 20 selected stations (locations are shown in Fig. 1b; the full list of stations is given in Table S1 of the supplementary materials). The RMSD is significantly reduced by the dynamical downscaling of AWI-CM1 data to the EUR-12 domain (see Table 1). In the case of the GER-3

https://doi.org/10.5194/esd-2024-16
Preprint. Discussion started: 15 July 2024
© Author(s) 2024. CC BY 4.0 License.

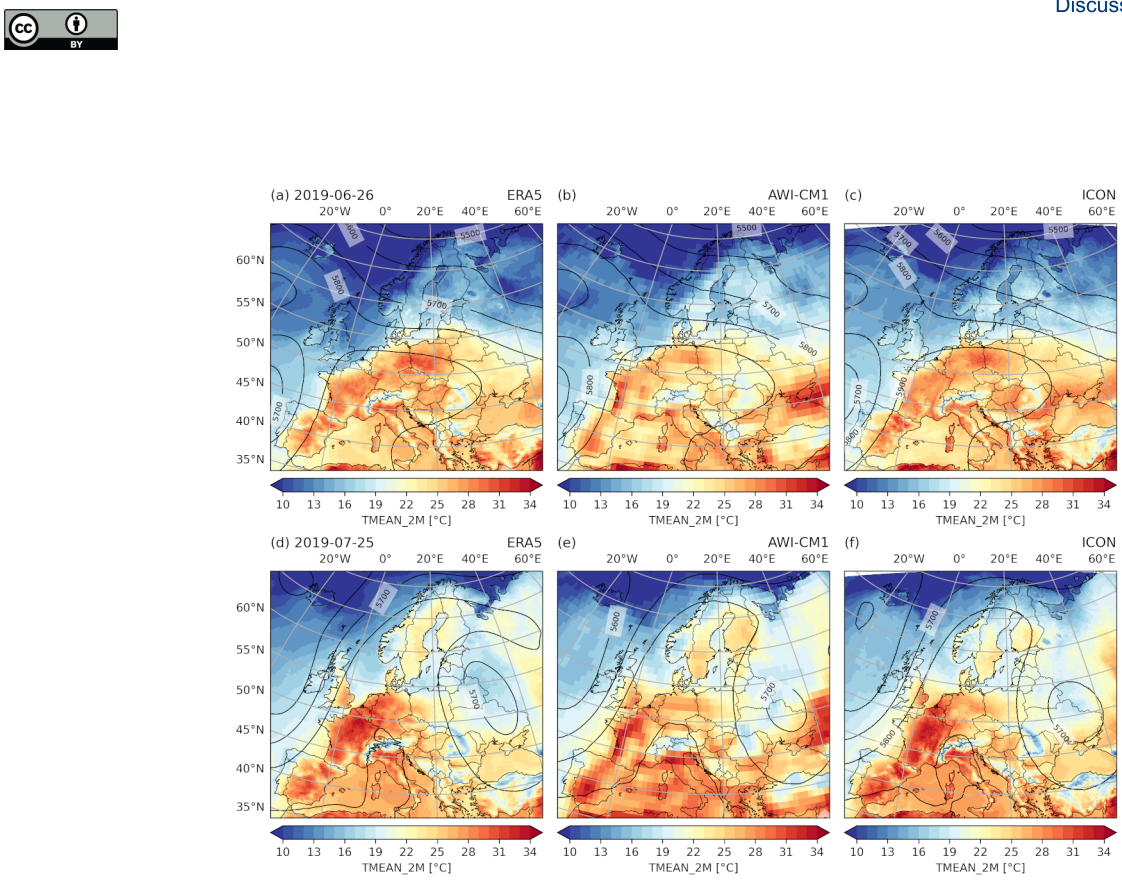

Figure 2. Mean 2m temperature (shading) and geopotential height at 500 hPa (contours) on 26.06.2019 (the first peak of the June heatwave) and 25.07.2019 (the peak of the July heatwave) for ERA5 (left), AWI-CM1 (middle), and ICON EUR-12 (right)

Table 1. The root mean square differences (RMSD) in °C of daily maximum, mean, and minimum 2m temperature to DWD station observations during summer (June to August) 2019 averaged over 20 stations (for locations, see Fig. 1)

	AWI-CM1	ICON EUR-12	ICON GER-3
TMAX_2M	3.99 (σ=1.35)	2.88 (σ=0.62)	2.79 (σ=0.46)
TMEAN_2M	2.20 (σ=1.24)	1.66 (σ=0.45)	1.73 (σ=0.50)
TMIN_2M	3.21 (σ=1.08)	2.37 (σ=0.62)	2.67 (σ=0.43)

simulation, a further reduction of the RMSD could be achieved only for the daily maximum 2m temperatures, whereas daily minimum and mean temperatures slightly deteriorated but remained clearly improved relative to AWI-CM1. A similar result can be obtained when the RMSD is calculated between the simulations and E-OBS time series shown in Fig. 3 (RMSD values in the legend).

Figure 4a,d,g shows the spatial distribution of RMSD for EUR-12 with respect to E-OBS for daily maximum, mean, and minimum temperatures during the summer of 2019. The RMSD varies between 1 and 2 °C in Central Europe for the daily mean temperature and between 2 and 3.5 °C for the daily minimum and maximum temperatures, which supports the values shown in Table 1. To assess the added value of our regional simulations, we interpolated the ICON EUR-12 data to the grid

https://doi.org/10.5194/esd-2024-16
Preprint. Discussion started: 15 July 2024
© Author(s) 2024. CC BY 4.0 License.

Earth System Dynamics
Discussions
Open Access
EGU

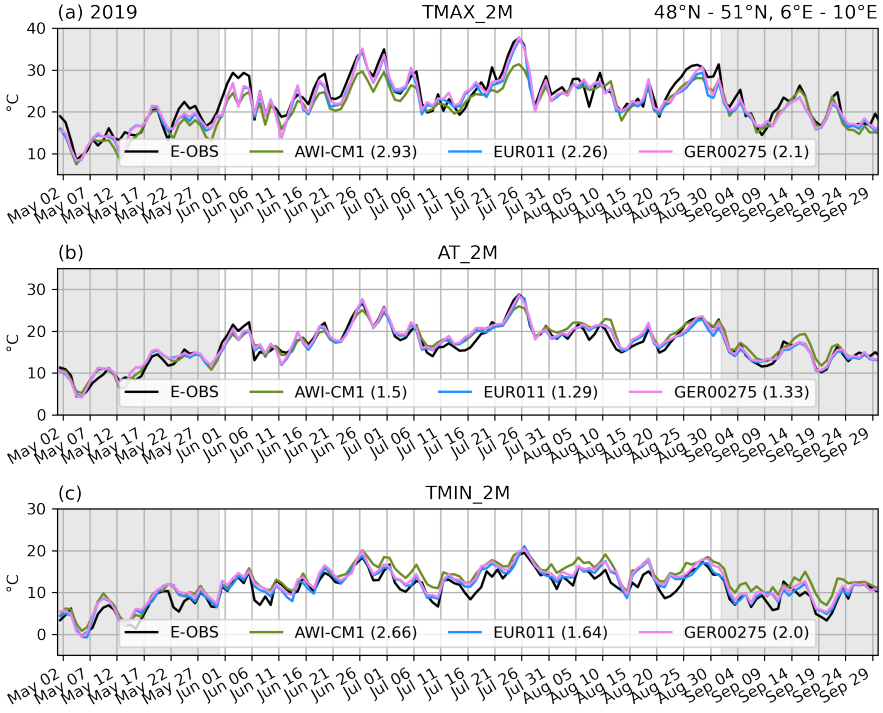

Figure 3. Comparison to E-OBS of (a) daily maximum, (b) daily mean, and (c) daily minimum 2m temperatures obtained with AWI-CM1, ICON EUR-12, and ICON GER-3 averaged across the longitude/latitude box with the boundaries 48° N - 51° N, 6° E - 10° E (dashed box in Fig. 1b). The numbers in brackets in the legend reflect the RMSD to E-OBS in June,July, and August.

of AWI-CM1 and compared the RMSD of both models to E-OBS. Green colours in Fig. 4b,e,h indicate an improvement in the performance of the regional simulations compared to the global AWI-CM1 simulation for the respective temperatures. The overall improvement in central and southern Europe is robust, with the exception of the maximum temperature at the coast of the Iberian Peninsula and north of the Black Sea.

To identify potential systematic biases, the observed E-OBS temperature fields were subtracted from the EUR-12 ones (see Fig. 4c,f,i). The original seasonally averaged temperatures can be found in Fig. S2. Our analysis revealed a pronounced positive bias of maximum temperatures in the areas where the RMSD increased in comparison to AWI-CM1. However, as our study is focused on Central Europe, the model performance in the most western and eastern parts of the domain is found to be acceptable. A similar analysis was conducted for all simulated summer seasons between 2018 and 2022 (Fig. S3). It demonstrates that the bias patterns persist consistently across all the simulated summers, indicating that the errors are not flow-dependent.

The added value of the nested convective-permitting GER-3 simulation is assessed by comparing the RMSD of the 2m temperature to observations with the RMSD of the driving EUR-12 simulation (see Fig. 5, first and second columns). With this aim, both temperature datasets were interpolated to the E-OBS grid (0.1° horizontal resolution). We also evaluated the

https://doi.org/10.5194/esd-2024-16
Preprint. Discussion started: 15 July 2024
© Author(s) 2024. CC BY 4.0 License.

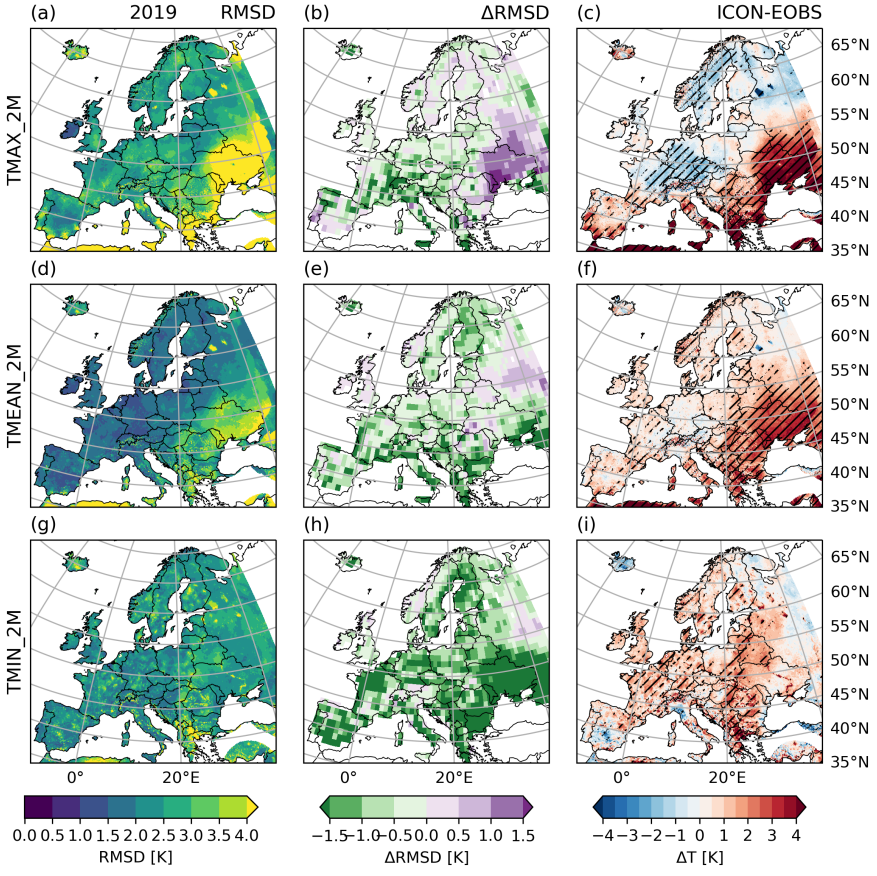

Figure 4. Added value assessment of the ICON EUR-12 simulation for June, July, August 2019 for daily (a-c) maximum, (d-f) mean, and (g-i) minimum 2m temperature. Left column: root mean square difference (RMSD) of the simulated daily 2m temperatures by ICON EUR-12 to E-OBS. Middle column: Change in RMSD achieved by dynamical downscaling; the green colours correspond to the reduced squared error of daily temperatures. Right column: seasonal mean bias with respect to E-OBS; in hatched areas, the difference of ICON EUR011 to E-OBS exceeds the E-OBS ensemble spread.

https://doi.org/10.5194/esd-2024-16
Preprint. Discussion started: 15 July 2024
© Author(s) 2024. CC BY 4.0 License.

Earth System Dynamics
Discussions
Open Access
EGU

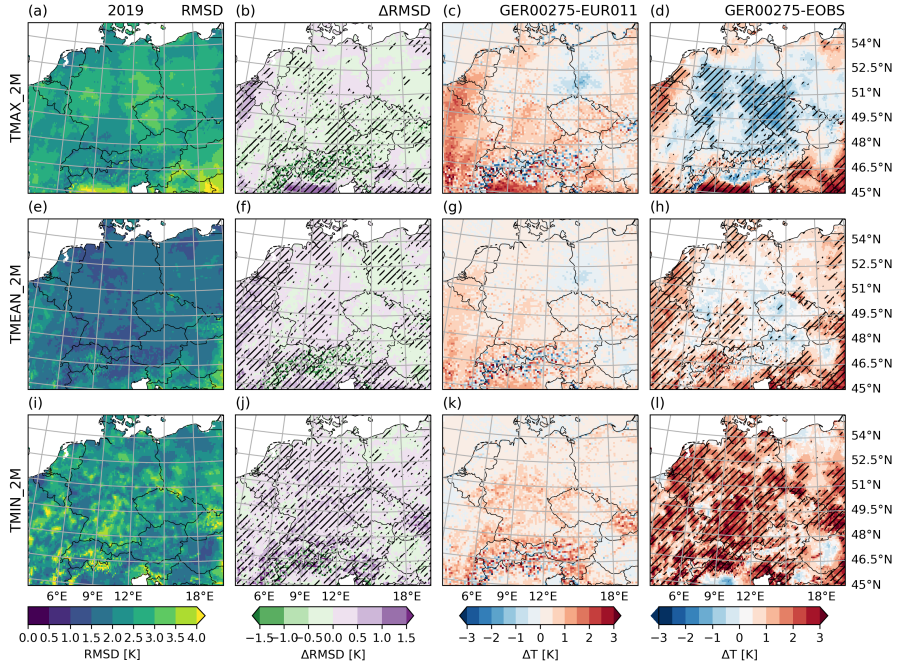

Figure 5. Added value assessment of the nested convective-permitting GER-3 simulation for June, July, August 2019 for daily (a-d) maximum, (e-h) mean, and (i-l) minimum 2m temperature. First column: root mean square difference (RMSD) of daily 2m temperature to E-OBS of the GER-3 simulation. Second column: Change of RMSD compared to the EUR-12 simulation (significant difference hatched, $p<0.05$). Third column: seasonal mean bias of the GER-3 simulation w.r.t. EUR-12. Fourth column: seasonal mean bias of the GER-3 simulation w.r.t E-OBS, hatching signifies the exceedance of the E-OBS ensemble spread

average bias between the nested simulations by subtracting the EUR-12 seasonal mean temperature fields from the GER-3 fields coarsened to the EUR-12 domain (see Fig. 5, third column), as well as the bias of the GER-3 fields with respect to E-OBS (Fig. 5, fourth column)

The nested GER-3 simulation is between 0.5 and 2 K warmer than the EUR-12, which reduces the negative bias of the daily maximum temperature over Germany, indicating a further added value of our approach. However, the positive bias of the daily minimum temperature increases, and the daily mean temperature representation shows no significant improvement over Germany. The most substantial bias of daily maximum temperature occurred in the western part of the domain over land (see Fig. 5 c,d). Due to improved topography, the nesting significantly reduced the RMSD of maximum and mean 2m temperature over the Alps (see Fig. 5 b,f).

Analogue to the EUR-12 simulation, the added value assessment of GER-3 simulation over the full simulation period yields that the patterns shown in Fig.5 remain consistent over the years for all modelled summer seasons between 2018 and 2022 (see Fig. S4 in supplementary materials), with a more prominent improvement of RMSD for the maximum temperatures (Fig. 5b and S4b).

https://doi.org/10.5194/esd-2024-16
Preprint. Discussion started: 15 July 2024
© Author(s) 2024. CC BY 4.0 License.

Earth System Dynamics Discussions
Open Access
EGU

3.2 Storylines for the summer 2019 heatwaves

Given the added value of dynamical downscaling with ICON-CLM for present-day conditions, we now analyse the regionalised past and future analogues of the July 2019 European heatwave.

We first consider the period corresponding to the peak of the July 2019 heatwave. According to Fig. 6, the maximum temperature on the 25th of July would exceed 40 °C over a considerable area of Western Europe for a +4 K climate. The area affected by temperatures exceeding 40 °C is projected to increase significantly in the EUR-12 simulations, from 20,000 km^2 in the pre-industrial climate to 290,000 km^2 in the present-day and 1,000,000 km^2 in the +4 K climate. Moreover, the 45 °C threshold would be exceeded over a large area in Western France already in a +3 K climate, and for the Benelux and Rhine valley in a +4 K warmer world (Fig. 6i and j).

The increase of the 2m temperature is not spatially homogeneous, with the regions located to the east of the heatwave's core experiencing stronger warming, thereby contributing to the increasing spatial extent of the heat wave. This is exemplified in Fig. S5, where the maximum temperature differences between the +4 K and pre-industrial climates reach 12 °C in Luxembourg, Southern Belgium, Western Germany, and the most eastern parts of France. The temperature increase in the core of the heatwave is close to 8 °C, which corresponds to a doubling of the global warming level (+4 K).

Figure 7 displays the time series of daily maximum, mean, and minimum temperatures averaged over a longitude/latitude area 48° N - 51° N and 6° E - 10° E (depicted in Fig. 1b) for the extended summer season (May to September) of 2019. During July and August, an increase in spread is found between the temperature curves corresponding to the different warming levels. Conversely, the spread between the time series of temperatures is much smaller in May and early June. This finding was previously confirmed in the analyses of the global storylines by Sánchez-Benítez et al. (2022) and will be further explored in the following section. We also see a larger spread in daily maximum curves in July and August compared to the mean and minimum temperatures.

3.3 Temperature scaling in response to global warming

In order to gain a deeper insight into the spread of temperature curves depicted in Fig. 7 and to address the question of temperature scaling in response to global warming, three five-day periods were selected for detailed analysis (highlighted orange in Fig. 7). The first period is in mid-June, when no heatwave was observed, while the second period is in late June during the first heatwave, and the third period is around the peak of the July heatwave. The daily maximum, mean, and minimum 2m temperatures averaged spatially over the area 48° N - 51° N, 6° E - 10° E and temporally over those periods show a clear linear dependency with the global warming level (see Fig. 8a-c). Therefore, we express anthropogenic change to the 2m temperatures per 1 °C of global warming as a slope of this line. This slope will be referred to in the following text as the "warming rate."

As shown in Fig. 8a, the average warming rate over the studied area is close to a factor of 1 in mid-June for all three curves. This indicates that the warming rate is comparable to global warming in the absence of an extreme event. The warming rates increase during the first heatwave and approach or even exceed a factor of 2 for maximum temperature during the July heatwave

https://doi.org/10.5194/esd-2024-16
Preprint. Discussion started: 15 July 2024
© Author(s) 2024. CC BY 4.0 License.

Earth System Dynamics
Discussions
Open Access
EGU

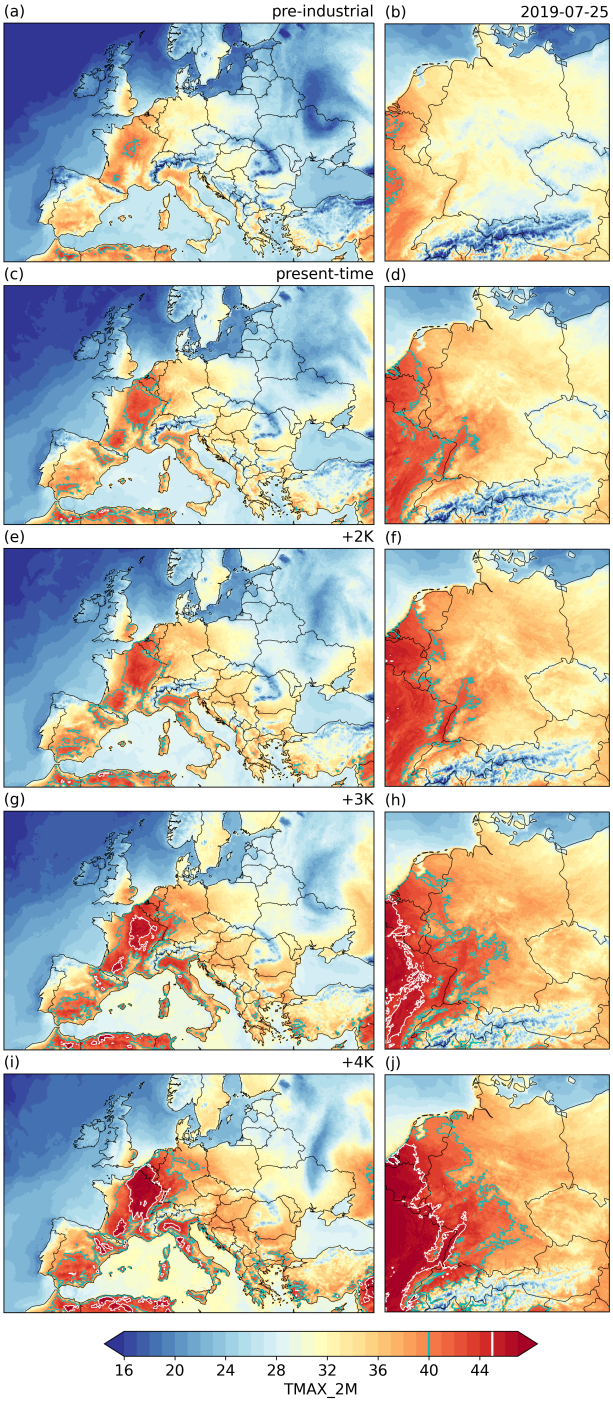

Figure 6. Daily maximum 2m temperature on the 25th of July as of the (left column) ICON EUR-12 simulations and (right column) ICON GER-3 simulations in pre-industrial (a, b), present-time (c, d), +2 K (e, f), +3 K (g, h), and +4 K (i, j) climates.

https://doi.org/10.5194/esd-2024-16
Preprint. Discussion started: 15 July 2024
© Author(s) 2024. CC BY 4.0 License.

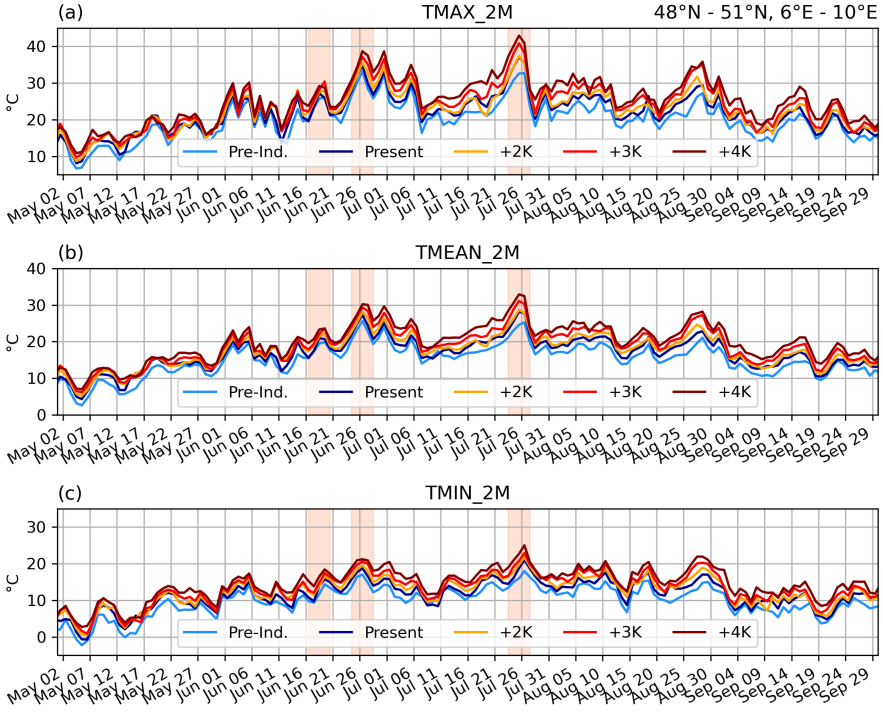

Figure 7. Daily (a) maximum, (b) mean, and (c) minimum temperatures averaged over the longitude/latitude box with boundaries 48° N - 51° N and 6° E - 10° E (see Fig. 1b) over the MJJAS period of the year 2019 based on the EUR-12 storyline simulations. The three highlighted periods (orange) are discussed in detail in section 3.3. For the GER-3 simulations, see Fig. S6

(Fig. 8b,c). This suggests that the expected differences for the maximum temperature for a similar event in a future climate would be exacerbated and be twice as high as the corresponding global warming level.

Using this method, we computed the individual temperature warming rates for a 5-day running mean (see Fig. 8d) for the extended summer season of 2019. Between May and early June, the warming rates fluctuate around 1. The values increase with the onset of the first heatwave in late June, with the maximum temperature responding stronger than the minimum temperature. Following a relative minimum in mid-July, the warming rates strongly increase before the 25th of July, reaching a factor of 2.2 for maximum temperature ahead and during the late July heat wave. After a short decrease directly after the temperature maximum, the warming rates increase again to values over 2 at the beginning of August. This is followed by a gradual decrease before the last peak of warming rates, which occurs in late August when the temperature again increases during the summer.

To comment on the broader warming rate peak ahead of the July heatwave that can be seen in Fig. 8d, we estimate the duration of this heatwave in different climates based on the exceedance of the 90th percentile of the modelled maximum 2m temperature, which is 30 °C when computed for all days in July over the simulated period of 2018-2022. According to our estimation, the duration of this heatwave would grow highly non-linearly from 4 days in the present-day climate to 5 days in the +3 K climate, and to 9 days in the +4 K warmer world (not shown).

https://doi.org/10.5194/esd-2024-16
Preprint. Discussion started: 15 July 2024
© Author(s) 2024. CC BY 4.0 License.

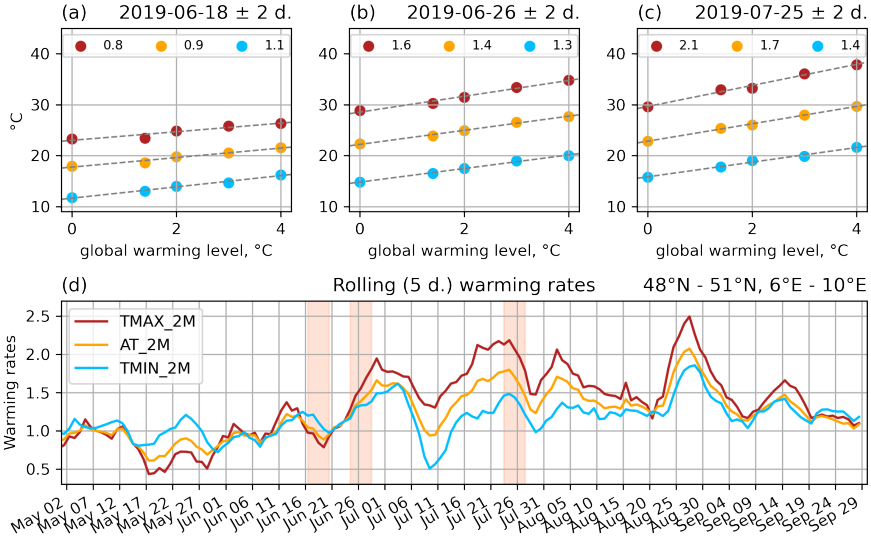

Figure 8. (a-c) Daily maximum (red), mean (orange), and minimum (blue) 2m temperature over the longitude/latitude box 48° N - 51° N, 6° E - 10° E averaged over three 5-day periods plotted against the global warming level. The numbers in the legend represent the slopes of the respective lines; (d) warming rates for the rolling average (5-day window) of daily maximum, mean, and minimum temperatures over the same box. The three highlighted periods are discussed in detail in section 3.3. Based on the EUR-12 simulation. For the GER-3 simulation, see Fig. S7

While the response of the maximum temperature in May and June is smaller or comparable to the response of the mean and minimum temperatures, the warming rate for the maximum temperature is very large during July and August. Thus, with global warming, the diurnal temperature range tends to increase in the mid and late summer of 2019. In contrast, the temperature response appears to be distributed more uniformly during the day in spring and early summer.

The warming rates are now computed for each grid point in the study area. Figure 9a displays the warming rates during the five-day period around the peak of the heatwave in late July 2019 (the third shaded area in Fig. 7) at each grid point in both the EUR-12 and GER-3 domains. According to the R2 maps in Fig. S8, the assumption of linear growth in the areas affected by the heatwave is valid in all cases.

The warming rates for the daily maximum temperatures exceed a factor of 2 over large areas in central and southern Europe (see Fig. 9a). In contrast, the minimum temperatures increase at a comparatively lower rate. This also indicates an enhanced diurnal temperature range during extreme heat events, as discussed above. Consistent with the values shown in Fig. 8a, the warming rates during a “neutral” period in early summer are much lower and below a factor of 1 across Central Europe (Fig. S9a).

A closer look into the response of the 2m temperature on the 25th of July reveals that the warming rates during the peak of the event reach a factor of 3.0 east of the heatwave’s core, in line with the finding that those areas would become up to 12 °C warmer in the +4 K climate compared to the pre-industrial time (see Fig. 9b). Accordingly, the spatial extent of the heatwave is

https://doi.org/10.5194/esd-2024-16
Preprint. Discussion started: 15 July 2024
© Author(s) 2024. CC BY 4.0 License.

Earth System Dynamics
Discussions
Open Access
EGU

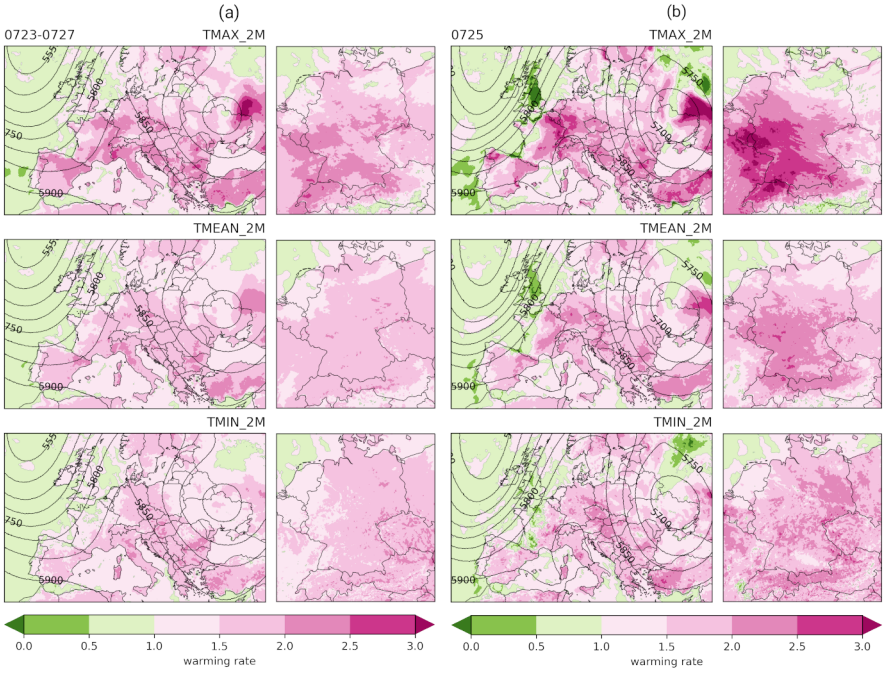

Figure 9. (a) Warming rates for the period from the 23rd to the 27th of July 2019. (b) Warming rates for the 25th of July. Contours: geopotential height as of the EUR-12 simulation.

subject to a rapid increase in future climates. As shown in Fig. S10, the area affected by the maximum temperatures over 40 °C on the 25th of July also grows linearly with the global warming level, with a rate of 250,000 km^2K^{-1}. The lack of warming over the British Isles may be explained by the fact that this area is located at the edge of the subtropical ridge triggering this event and, thus, less affected.

To compare the scaling of the temperatures during the extreme event to the mean summer scaling, we estimated the average response of the 2m temperatures over Europe for the total simulated period, which included five summers from 2018 to 2022. According to Fig. S11, the warming rate is smoothly distributed and stays below a factor of two over the whole continent, except for TMAX in several regions of Southern Europe. Figure 10 shows that the average temperature response for the summer of 2019 is similar to the multi-year mean. Nevertheless, it is worth mentioning that all the years of the simulated period lay within the European multi-year drought and heat event of 2018-2022 (Knutzen et al., 2023). Thus, the average warming rate in Fig. S11 may be higher than that for the years unaffected by severe drought conditions.

https://doi.org/10.5194/esd-2024-16
Preprint. Discussion started: 15 July 2024
© Author(s) 2024. CC BY 4.0 License.

Earth System Dynamics
Discussions
Open Access
EGU

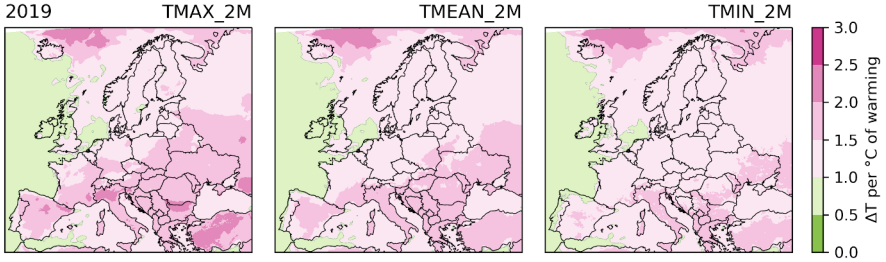

Figure 10. Warming rates for the mean summer 2m temperature in the year 2019 based on the EUR-12 storylines.

4 Summary and Discussion

In this study, we follow an event-based storyline approach using a GCM-RCM-CPM model chain to analyse the thermodynamic response of the European summer 2019 heatwaves to global warming. We obtained our storylines using spectral nudged global AWI-CM1 simulation and subsequent dynamical downscaling with the regional model ICON-CLM to resolutions of 12 km (EUR-12) and 3 km (GER-3).

The outcomes of the simulations permit the answering of the three key research questions:

(1) How accurately can a regional event-based storyline simulation represent a recent event, and what is the added value compared to the global spectral nudged storyline simulation?

The daily spatial and temporal patterns of the 2m temperature fields obtained with the AWI-CM1 - ICON model chain show good agreement with ERA5, E-OBS, and DWD station observations for the summer of 2019. Compared to the driving AWI-CM1 simulations, the dynamical downscaling significantly reduced the RMSD of 2m temperature over most of Europe (by about 1.5 °C in Central Europe). The GER-3 simulation gives even more spatial details to the EUR-12 for the daily maximum temperature.

(2) What is the effect of climate change on the 2019 European heatwave based on the regional and convective-permitting ICON-CLM simulations?

Based on the simulations for our case study in 2019 with different thresholds for global warming, the peak temperatures of the July heatwave would increase considerably beyond the underlying global warming level, with the magnitude of the temperature response depending on the location. The increments of daily maximum temperature in the +4 K climate with respect to the pre-industrial climate vary between 8 °C in the centre of the heatwave and 12 °C to the west of it. This leads to the increased spatial extent of the heatwave in the warmer world. In the context of the present-day climate, where we took the 40 °C isoline as a benchmark, the affected area would be encompassed by the 45 °C isoline in a +4 K world. Consequently, the areas affected by temperatures exceeding 40 °C would experience a significant expansion, increasing from 290,000 km^2 in the present-day to 1,000,000 km^2 in the +4 K storyline. When considering the time series of 2m temperature over the area 48° N - 51° N, 6° E - 10° E for all five storylines, the spread between the curves appeared to be higher in mid and late summer

https://doi.org/10.5194/esd-2024-16
Preprint. Discussion started: 15 July 2024
© Author(s) 2024. CC BY 4.0 License.


compared to the early summer. This aligns with the previous findings that suggest intraseasonal dependency of anthropogenic warming based not only on the nudged storylines but also on the free CMIP6 runs (Sánchez-Benítez et al., 2022).

(3) What is the local to regional extreme temperature scaling in response to global warming for an event like the 2019 heat wave, and how does it differ from the scaling of the global mean temperature?

Our findings reveal a linear dependency of the 2m temperature response to the global warming level, with the observed warming rate determined by the slope of the linear regression demonstrating spatial and temporal variations. Quantifying the smaller spacing between the temperature curves mentioned above, the warming rates over the studied area in the early summer fluctuate around 1, indicating that regional warming aligns with global warming for that period. However, in July and August, the warming rates for daily maximum temperatures vary between 1.5 and 2.5, reaching higher values with each successive heatwave during the study period (see Fig. 8d).

Furthermore, the broadening of the warming rate peak during the July heatwave means extending the heatwave's duration in a warmer world. We also observe the broadening of the diurnal temperature range in future climates, which is indicated by much lower warming rates for the minimum temperature than those for the daily maximum. This difference does not occur in early summer and disappears again by late September. Considering that the first heatwave in late June had modified the soil moisture for the rest of the summer (Sousa et al., 2020; Sánchez-Benítez et al., 2022), this case exemplifies the dependency of the global warming amplification on the event-specific regional evolution of the thermodynamic conditions.

On the 25th of July, the response of the maximum 2m temperature (warming rate) reached a factor of 3 in some areas (Fig. 9b). However, the highest warming rates are not located over the heatwave centre but instead shifted eastward (Fig. S4). The areas less affected by unprecedented temperatures but still located within the influence of the event triggered by the subtropical ridge tend to heat stronger in the warmer world. Thus, along with the increasing duration, the area affected by the heatwave is expanding. We estimated that on the 25th of July, the area with maximum temperatures exceeding 40 °C in Europe would increase at the rate of 250,000 km^2K^{-1}.

The high but limited (<2.5 on the 25th of July) warming rates at the centre of the July 2019 heatwave may be explained by a physical limitation of maximal reachable near-surface temperatures and the possible decrease in the strength of soil moisture-temperature coupling over desiccated soils (e.g., Zhang and Boos, 2023; Gevaert et al., 2018). Meanwhile, regions east of the heatwave centre may enter a different coupling regime, leading to an amplified response of near-surface temperature to decreasing soil moisture (Gevaert et al., 2018; Miralles et al., 2014). The overall amplification of the warming rates during the heatwave events and the extension of the diurnal temperature range may likewise be exacerbated due to soil-atmosphere feedback. However, further exploration of those mechanisms is out of the scope of this paper and is considered the main direction of future research.

5 Conclusions

The aim of this study was to provide a regional perspective of the global spectral nudged storylines for the summer heatwaves of 2019 in Central Europe. To our best knowledge, we addressed here for the first time the unfolding of the heatwaves on

https://doi.org/10.5194/esd-2024-16
Preprint. Discussion started: 15 July 2024
© Author(s) 2024. CC BY 4.0 License.


the regional-to-local spatial scales and followed the evolution of the near-surface temperatures throughout the whole summer season in five dynamical analogues of the summer of 2019 by a dynamical downscaling approach. We observed that the late June heatwave triggered higher warming rates and an extension of the diurnal temperature range in a warmer world for the rest of the summer. Additionally, we obtained the higher warming rates over the regions east of the July heatwave centre, as well as the broadening of the warming rate peaks associated with both 2019 heatwaves. This demonstrates that our approach allows not only for the estimation of possible impacts of extreme heat events in the warmer world but also for the investigation of the mechanisms and conditions that lead to different rates of response to background warming.

Our regional storylines can be used to drive hydrology, land surface, and other impact models that will deliver relevant information for developing adaptation measures. Finally, the insights gained from storyline-based regional impact studies are more tangible than probabilistic estimates and, thus, bear the potential to raise public awareness about the significance of the effects of climate change on the community level.

Code and data availability. The ICON model is available as open source release since January 2024 under https://icon-model.org/. The runtime environment SPICE v.2.0 is available online under https://zenodo.org/records/6838984. The simulations are stored on the supercomputer Levante at the German Climate Computation Center (DKRZ, Hamburg) and will be made available online upon completion of the data preparation. ERA5 data can be downloaded from the Copernicus Climate Change Service (C3S) Climate Date Store (https://cds.climate.copernicus.eu) and can be accessed at the DKRZ by the users of the Levante HPC system. The E-OBS dataset can be accessed at the website of the European Climate Assessment & Dataset project (https://www.ecad.eu/download/ensembles/download.php). The DWD station data are freely available for research at the Open Data Portal of the German Weather Service DWD (https://opendata.dwd.de, DWD, 2023).

Author contributions. TK, PL and JGP conceived and designed the study. ASB computed the global AWI-CM1 simulations and provided the data and necessary instructions. PL took care of the pre-processing of the input data to ICON. TK performed the ICON simulations with the help of PL, performed the data analysis and prepared the figures. HG and PB contributed additional modelling expertise. TK wrote the initial paper draft. All authors discussed the results and contributed with manuscript revisions.

Competing interests. The contact author has declared that none of the authors has any competing interests.

Acknowledgements. This work was supported by funding from the Helmholtz Research Field Earth & Environment for the Innovation Pool Project SCENIC. JGP thanks the AXA research fund for support. The authors thank the German Climate Computation Center (DKRZ, Hamburg) for providing computing and storage resources under projects 105 and 1264. The global AWI-CM1 simulations were performed using ESM Tools (Barbi et al., 2021). The authors further thank Klaus Keuler for providing the ICON-CLM settings and domain grids used

https://doi.org/10.5194/esd-2024-16
Preprint. Discussion started: 15 July 2024
© Author(s) 2024. CC BY 4.0 License.

Earth System Dynamics Discussions
Open Access
EGU

within the NUKLEUS project and Florian Ehmele for establishing the workflow of the dynamical downscaling and producing the set of preliminary simulations.

https://doi.org/10.5194/esd-2024-16
Preprint. Discussion started: 15 July 2024
© Author(s) 2024. CC BY 4.0 License.

References

Athanase, M., Sánchez-Benítez, A., Goessling, H. F., Pithan, F., and Jung, T.: Projected amplification of summer marine heatwaves in a warming Northeast Pacific Ocean, Communications Earth & Environment, 5, 1–12, https://doi.org/10.1038/s43247-024-01212-1, number: 1 Publisher: Nature Publishing Group, 2024.

Barbi, D., Wieters, N., Gierz, P., Andrés-Martínez, M., Ural, D., Chegini, F., Khosravi, S., and Cristini, L.: ESM-Tools version 5.0: a modular infrastructure for stand-alone and coupled Earth system modelling (ESM), Geoscientific Model Development, 14, 4051–4067, https://doi.org/10.5194/gmd-14-4051-2021, publisher: Copernicus GmbH, 2021.

Barriopedro, D., Fischer, E. M., Luterbacher, J., Trigo, R. M., and García-Herrera, R.: The Hot Summer of 2010: Redrawing the Temperature Record Map of Europe, Science, 332, 220–224, https://doi.org/10.1126/science.1201224, publisher: American Association for the Advancement of Science, 2011.

Barriopedro, D., García-Herrera, R., Ordóñez, C., Miralles, D. G., and Salcedo-Sanz, S.: Heat Waves: Physical Understanding and Scientific Challenges, Reviews of Geophysics, 61, e2022RG000 780, https://doi.org/10.1029/2022RG000780, _eprint: https://onlinelibrary.wiley.com/doi/pdf/10.1029/2022RG000780, 2023.

Becker, F. N., Fink, A. H., Bissolli, P., and Pinto, J. G.: Towards a more comprehensive assessment of the intensity of historical European heat waves (1979–2019), Atmospheric Science Letters, 23, e1120, https://doi.org/10.1002/asl.1120, _eprint: https://onlinelibrary.wiley.com/doi/pdf/10.1002/asl.1120, 2022.

Calvin, K., Dasgupta, D., Krinner, G., Mukherji, A., Thorne, P. W., Trisos, C., Romero, J., Aldunce, P., Barrett, K., Blanco, G., Cheung, W. W., Connors, S., Denton, F., Diongue-Niang, A., Dodman, D., Garschagen, M., Geden, O., Hayward, B., Jones, C., Jotzo, F., Krug, T., Lasco, R., Lee, Y.-Y., Masson-Delmotte, V., Meinshausen, M., Mintenbeck, K., Mokssit, A., Otto, F. E., Pathak, M., Pirani, A., Poloczanska, E., Pörtner, H.-O., Revi, A., Roberts, D. C., Roy, J., Ruane, A. C., Skea, J., Shukla, P. R., Slade, R., Slangen, A., Sokona, Y., Sörensson, A. A., Tignor, M., Van Vuuren, D., Wei, Y.-M., Winkler, H., Zhai, P., Zommers, Z., Hourcade, J.-C., Johnson, F. X., Pachauri, S., Simpson, N. P., Singh, C., Thomas, A., Totin, E., Arias, P., Bustamante, M., Elgizouli, I., Flato, G., Howden, M., Méndez-Vallejo, C., Pereira, J. J., Pichs-Madruga, R., Rose, S. K., Saheb, Y., Sánchez Rodríguez, R., Ürge Vorsatz, D., Xiao, C., Yassaa, N., Alegría, A., Armour, K., Bednar-Friedl, B., Blok, K., Cissé, G., Dentener, F., Eriksen, S., Fischer, E., Garner, G., Guivarch, C., Haasnoot, M., Hansen, G., Hauser, M., Hawkins, E., Hermans, T., Kopp, R., Leprince-Ringuet, N., Lewis, J., Ley, D., Ludden, C., Niamir, L., Nicholls, Z., Some, S., Szopa, S., Trewin, B., Van Der Wijst, K.-I., Winter, G., Witting, M., Birt, A., Ha, M., Romero, J., Kim, J., Haites, E. F., Jung, Y., Stavins, R., Birt, A., Ha, M., Orendain, D. J. A., Ignon, L., Park, S., Park, Y., Reisinger, A., Cammaramo, D., Fischlin, A., Fuglestvedt, J. S., Hansen, G., Ludden, C., Masson-Delmotte, V., Matthews, J. R., Mintenbeck, K., Pirani, A., Poloczanska, E., Leprince-Ringuet, N., and Péan, C.: IPCC, 2023: Climate Change 2023: Synthesis Report. Contribution of Working Groups I, II and III to the Sixth Assessment Report of the Intergovernmental Panel on Climate Change [Core Writing Team, H. Lee and J. Romero (eds.)]. IPCC, Geneva, Switzerland., Tech. rep., Intergovernmental Panel on Climate Change (IPCC), https://doi.org/10.59327/IPCC/AR6-9789291691647, edition: First, 2023.

Cornes, R. C., van der Schrier, G., van den Besselaar, E. J. M., and Jones, P. D.: An Ensemble Version of the E-OBS Temperature and Precipitation Data Sets, Journal of Geophysical Research: Atmospheres, 123, 9391–9409, https://doi.org/10.1029/2017JD028200, _eprint: https://onlinelibrary.wiley.com/doi/pdf/10.1029/2017JD028200, 2018.

Deser, C., Phillips, A. S., Alexander, M. A., and Smoliak, B. V.: Projecting North American Climate over the Next 50 Years: Uncertainty due to Internal Variability, Journal of Climate, 27, 2271–2296, https://doi.org/10.1175/JCLI-D-13-00451.1, publisher: American Meteorological Society Section: Journal of Climate, 2014.

https://doi.org/10.5194/esd-2024-16
Preprint. Discussion started: 15 July 2024
© Author(s) 2024. CC BY 4.0 License.

DWD: Historical Daily Station Observations (Temperature, Pressure, Precipitation, Sunshine Duration, etc.) for Germany, Version v23.3, https://opendata.dwd.de/climate_environment/CDC/observations_germany/climate/daily/kl/historical/, last access: [15.03.2024], 2023.

Eyring, V., Bony, S., Meehl, G. A., Senior, C. A., Stevens, B., Stouffer, R. J., and Taylor, K. E.: Overview of the Coupled Model Intercomparison Project Phase 6 (CMIP6) experimental design and organization, Geoscientific Model Development, 9, 1937–1958, https://doi.org/10.5194/gmd-9-1937-2016, publisher: Copernicus GmbH, 2016.

Feser, F., Rockel, B., Storch, H. v., Winterfeldt, J., and Zahn, M.: Regional Climate Models Add Value to Global Model Data: A Review and Selected Examples, Bulletin of the American Meteorological Society, 92, 1181–1192, https://doi.org/10.1175/2011BAMS3061.1, publisher: American Meteorological Society Section: Bulletin of the American Meteorological Society, 2011.

Fink, A. H., Brücher, T., Krüger, A., Leckebusch, G. C., Pinto, J. G., and Ulbrich, U.: The 2003 European summer heatwaves and drought –synoptic diagnosis and impacts, Weather, 59, 209–216, https://doi.org/10.1256/wea.73.04, 2004.

García-Herrera, R., Díaz, J., Trigo, R. M., Luterbacher, J., and Fischer, E. M.: A Review of the European Summer Heat Wave of 2003, Critical Reviews in Environmental Science and Technology, 40, 267–306, https://doi.org/10.1080/10643380802238137, publisher: Taylor & Francis _eprint: https://doi.org/10.1080/10643380802238137, 2010.

Gevaert, A. I., Miralles, D. G., de Jeu, R. a. M., Schellekens, J., and Dolman, A. J.: Soil Moisture-Temperature Coupling in a Set of Land Surface Models, Journal of Geophysical Research: Atmospheres, 123, 1481–1498, https://doi.org/10.1002/2017JD027346, _eprint: https://onlinelibrary.wiley.com/doi/pdf/10.1002/2017JD027346, 2018.

Giorgi, F.: Thirty Years of Regional Climate Modeling: Where Are We and Where Are We Going next?, Journal of Geophysical Research: Atmospheres, 124, 5696–5723, https://doi.org/10.1029/2018JD030094, _eprint: https://onlinelibrary.wiley.com/doi/pdf/10.1029/2018JD030094, 2019.

Giorgi, F. and Gutowski Jr, W. J.: Regional Dynamical Downscaling and the CORDEX Initiative, Annual Review of Environment and Resources, 40, 467–490, https://doi.org/10.1146/annurev-environ-102014-021217, publisher: Annual Reviews, 2015.

Hersbach, H., Bell, B., Berrisford, P., Hirahara, S., Horányi, A., Muñoz-Sabater, J., Nicolas, J., Peubey, C., Radu, R., Schepers, D., Simmons, A., Soci, C., Abdalla, S., Abellan, X., Balsamo, G., Bechtold, P., Biavati, G., Bidlot, J., Bonavita, M., De Chiara, G., Dahlgren, P., Dee, D., Diamantakis, M., Dragani, R., Flemming, J., Forbes, R., Fuentes, M., Geer, A., Haimberger, L., Healy, S., Hogan, R. J., Hólm, E., Janisková, M., Keeley, S., Laloyaux, P., Lopez, P., Lupu, C., Radnoti, G., de Rosnay, P., Rozum, I., Vamborg, F., Villaume, S., and Thépaut, J.-N.: The ERA5 global reanalysis, Quarterly Journal of the Royal Meteorological Society, 146, 1999–2049, https://doi.org/10.1002/qj.3803, _eprint: https://onlinelibrary.wiley.com/doi/pdf/10.1002/qj.3803, 2020.

Hundhausen, M., Feldmann, H., Laube, N., and Pinto, J. G.: Future heat extremes and impacts in a convection-permitting climate ensemble over Germany, Natural Hazards and Earth System Sciences, 23, 2873–2893, https://doi.org/10.5194/nhess-23-2873-2023, publisher: Copernicus GmbH, 2023.

Jacob, D., Petersen, J., Eggert, B., Alias, A., Christensen, O. B., Bouwer, L. M., Braun, A., Colette, A., Déqué, M., Georgievski, G., Georgopoulou, E., Gobiet, A., Menut, L., Nikulin, G., Haensler, A., Hempelmann, N., Jones, C., Keuler, K., Kovats, S., Kröner, N., Kotlarski, S., Kriegsmann, A., Martin, E., van Meijgaard, E., Moseley, C., Pfeifer, S., Preuschmann, S., Radermacher, C., Radtke, K., Rechid, D., Rounsevell, M., Samuelsson, P., Somot, S., Soussana, J.-F., Teichmann, C., Valentini, R., Vautard, R., Weber, B., and Yiou, P.: EURO-CORDEX: new high-resolution climate change projections for European impact research, Regional Environmental Change, 14, 563–578, https://doi.org/10.1007/s10113-013-0499-2, 2014.

https://doi.org/10.5194/esd-2024-16
Preprint. Discussion started: 15 July 2024
© Author(s) 2024. CC BY 4.0 License.

Kaspar, F., Müller-Westermeier, G., Penda, E., Mächel, H., Zimmermann, K., Kaiser-Weiss, A., and Deutschländer, T.: Monitoring of climate change in Germany – data, products and services of Germany's National Climate Data Centre, Advances in Science and Research, 10, 99–106, https://doi.org/10.5194/asr-10-99-2013, 2013.

Knutzen, F., Averbeck, P., Barrasso, C., Bouwer, L. M., Gardiner, B., Grünzweig, J. M., Hänel, S., Haustein, K., Johannessen, M. R., Kollet, S., Pietikaeinen, J.-P., Pietras-Couffignal, K., Pinto, J. G., Rechid, D., Rousi, E., Russo, A., Suarez-Gutierrez, L., Wendler, J., Xoplaki, E., and Gliksman, D.: Impacts and damages of the European multi-year drought and heat event 2018–2022 on forests, a review, EGUsphere, pp. 1–56, https://doi.org/10.5194/egusphere-2023-1463, publisher: Copernicus GmbH, 2023.

Miralles, D. G., Teuling, A. J., van Heerwaarden, C. C., and Vilà-Guerau de Arellano, J.: Mega-heatwave temperatures due to combined soil desiccation and atmospheric heat accumulation, Nature Geoscience, 7, 345–349, https://doi.org/10.1038/ngeo2141, number: 5 Publisher: Nature Publishing Group, 2014.

Perkins-Kirkpatrick, S. E. and Lewis, S. C.: Increasing trends in regional heatwaves, Nature Communications, 11, 3357, https://doi.org/10.1038/s41467-020-16970-7, 2020.

Pham, T. V., Steger, C., Rockel, B., Keuler, K., Kirchner, I., Mertens, M., Rieger, D., Zängl, G., and Früh, B.: ICON in Climate Limited-area Mode (ICON release version 2.6.1): a new regional climate model, Geoscientific Model Development, 14, 985–1005, https://doi.org/10.5194/gmd-14-985-2021, publisher: Copernicus GmbH, 2021.

Pithan, F., Athanase, M., Dahlke, S., Sánchez-Benítez, A., Shupe, M. D., Sledd, A., Streffing, J., Svensson, G., and Jung, T.: Nudging allows direct evaluation of coupled climate models with in situ observations: a case study from the MOSAiC expedition, Geoscientific Model Development, 16, 1857–1873, https://doi.org/10.5194/gmd-16-1857-2023, publisher: Copernicus GmbH, 2023.

Prein, A. F., Langhans, W., Fosser, G., Ferrone, A., Ban, N., Goergen, K., Keller, M., Tölle, M., Gutjahr, O., Feser, F., Brisson, E., Kollet, S., Schmidli, J., van Lipzig, N. P. M., and Leung, R.: A review on regional convection-permitting climate modeling: Demonstrations, prospects, and challenges, Reviews of Geophysics, 53, 323–361, https://doi.org/10.1002/2014RG000475, _eprint: https://onlinelibrary.wiley.com/doi/pdf/10.1002/2014RG000475, 2015.

Prill, F., Reinert, D., Rieger, D., and Zängl, G.: ICON Tutorial 2023: Working with the ICON Model, https://doi.org/10.5676/DWD_PUB/NWV/ICON_TUTORIAL2023, publisher: [DWD], 2023.

Robine, J.-M., Cheung, S. L. K., Le Roy, S., Van Oyen, H., Griffiths, C., Michel, J.-P., and Herrmann, F. R.: Death toll exceeded 70,000 in Europe during the summer of 2003, Comptes Rendus Biologies, 331, 171–178, https://doi.org/10.1016/j.crvi.2007.12.001, 2008.

Rockel, B. and Geyer, B.: SPICE (Starter Package for ICON-CLM Experiments), https://doi.org/10.5281/zenodo.6838984, 2022.

Rubin, D. B.: Matching to Remove Bias in Observational Studies, Biometrics, 29, 159–183, https://doi.org/10.2307/2529684, publisher: [Wiley, International Biometric Society], 1973.

Sein, D. V., Koldunov, N. V., Danilov, S., Wang, Q., Sidorenko, D., Fast, I., Rackow, T., Cabos, W., and Jung, T.: Ocean Modeling on a Mesh With Resolution Following the Local Rossby Radius, Journal of Advances in Modeling Earth Systems, 9, 2601–2614, https://doi.org/10.1002/2017MS001099, _eprint: https://onlinelibrary.wiley.com/doi/pdf/10.1002/2017MS001099, 2017.

Semmler, T., Danilov, S., Rackow, T., Sidorenko, D., Barbi, D., Hegewald, J., Pradhan, H. K., Sein, D., Wang, Q., and Jung, T.: AWI AWI-CM1.1MR model output prepared for CMIP6 ScenarioMIP ssp370, https://doi.org/10.22033/ESGF/CMIP6.2803, 2019.

Semmler, T., Danilov, S., Gierz, P., Goessling, H. F., Hegewald, J., Hinrichs, C., Koldunov, N., Khosravi, N., Mu, L., Rackow, T., Sein, D. V., Sidorenko, D., Wang, Q., and Jung, T.: Simulations for CMIP6 With the AWI Climate Model AWI-CM-1-1, Journal of Advances in Modeling Earth Systems, 12, e2019MS002 009, https://doi.org/10.1029/2019MS002009, _eprint: https://onlinelibrary.wiley.com/doi/pdf/10.1029/2019MS002009, 2020.

https://doi.org/10.5194/esd-2024-16
Preprint. Discussion started: 15 July 2024
© Author(s) 2024. CC BY 4.0 License.

Shepherd, T. G.: Atmospheric circulation as a source of uncertainty in climate change projections, Nature Geoscience, 7, 703–708, https://doi.org/10.1038/ngeo2253, number: 10 Publisher: Nature Publishing Group, 2014.

Shepherd, T. G.: Bringing physical reasoning into statistical practice in climate-change science, Climatic Change, 169, 2, https://doi.org/10.1007/s10584-021-03226-6, 2021.

Shepherd, T. G., Boyd, E., Calel, R. A., Chapman, S. C., Dessai, S., Dima-West, I. M., Fowler, H. J., James, R., Maraun, D., Martius, O., Senior, C. A., Sobel, A. H., Stainforth, D. A., Tett, S. F. B., Trenberth, K. E., van den Hurk, B. J. J. M., Watkins, N. W., Wilby, R. L., and Zenghelis, D. A.: Storylines: an alternative approach to representing uncertainty in physical aspects of climate change, Climatic Change, 151, 555–571, https://doi.org/10.1007/s10584-018-2317-9, 2018.

Sidorenko, D., Rackow, T., Jung, T., Semmler, T., Barbi, D., Danilov, S., Dethloff, K., Dorn, W., Fieg, K., Goessling, H. F., Handorf, D., Harig, S., Hiller, W., Juricke, S., Losch, M., Schröter, J., Sein, D. V., and Wang, Q.: Towards multi-resolution global climate modeling with ECHAM6–FESOM. Part I: model formulation and mean climate, Climate Dynamics, 44, 757–780, https://doi.org/10.1007/s00382-014-2290-6, 2015.

Sousa, P. M., Barriopedro, D., García-Herrera, R., Ordóñez, C., Soares, P. M. M., and Trigo, R. M.: Distinct influences of large-scale circulation and regional feedbacks in two exceptional 2019 European heatwaves, Communications Earth & Environment, 1, 1–13, https://doi.org/10.1038/s43247-020-00048-9, number: 1 Publisher: Nature Publishing Group, 2020.

Spensberger, C., Madonna, E., Boettcher, M., Grams, C. M., Papritz, L., Quinting, J. F., Röthlisberger, M., Sprenger, M., and Zschenderlein, P.: Dynamics of concurrent and sequential Central European and Scandinavian heatwaves, Quarterly Journal of the Royal Meteorological Society, 146, 2998–3013, https://doi.org/10.1002/qj.3822, _eprint: https://onlinelibrary.wiley.com/doi/pdf/10.1002/qj.3822, 2020.

Stevens, B., Giorgetta, M., Esch, M., Mauritsen, T., Crueger, T., Rast, S., Salzmann, M., Schmidt, H., Bader, J., Block, K., Brokopf, R., Fast, I., Kinne, S., Kornblueh, L., Lohmann, U., Pincus, R., Reichler, T., and Roeckner, E.: Atmospheric component of the MPI-M Earth System Model: ECHAM6, Journal of Advances in Modeling Earth Systems, 5, 146–172, https://doi.org/10.1002/jame.20015, _eprint: https://onlinelibrary.wiley.com/doi/pdf/10.1002/jame.20015, 2013.

Sánchez-Benítez, A., García-Herrera, R., Barriopedro, D., Sousa, P. M., and Trigo, R. M.: June 2017: The Earliest European Summer Mega-heatwave of Reanalysis Period, Geophysical Research Letters, 45, 1955–1962, https://doi.org/10.1002/2018GL077253, _eprint: https://onlinelibrary.wiley.com/doi/pdf/10.1002/2018GL077253, 2018.

Sánchez-Benítez, A., Goessling, H., Pithan, F., Semmler, T., and Jung, T.: The July 2019 European Heat Wave in a Warmer Climate: Storyline Scenarios with a Coupled Model Using Spectral Nudging, Journal of Climate, 35, 2373–2390, https://doi.org/10.1175/JCLI-D-21-0573.1, publisher: American Meteorological Society Section: Journal of Climate, 2022.

van Garderen, L., Feser, F., and Shepherd, T. G.: A methodology for attributing the role of climate change in extreme events: a global spectrally nudged storyline, Natural Hazards and Earth System Sciences, 21, 171–186, https://doi.org/10.5194/nhess-21-171-2021, publisher: Copernicus GmbH, 2021.

Vautard, R., Kadygrov, N., Iles, C., Boberg, F., Buonomo, E., Bülow, K., Coppola, E., Corre, L., van Meijgaard, E., Nogherotto, R., Sandstad, M., Schwingshackl, C., Somot, S., Aalbers, E., Christensen, O. B., Ciarlo, J. M., Demory, M.-E., Giorgi, F., Jacob, D., Jones, R. G., Keuler, K., Kjellström, E., Lenderink, G., Levavasseur, G., Nikulin, G., Sillmann, J., Solidoro, C., Sørland, S. L., Steger, C., Teichmann, C., Warrach-Sagi, K., and Wulfmeyer, V.: Evaluation of the Large EURO-CORDEX Regional Climate Model Ensemble, Journal of Geophysical Research: Atmospheres, 126, e2019JD032 344, https://doi.org/10.1029/2019JD032344, _eprint: https://onlinelibrary.wiley.com/doi/pdf/10.1029/2019JD032344, 2021.

https://doi.org/10.5194/esd-2024-16
Preprint. Discussion started: 15 July 2024
© Author(s) 2024. CC BY 4.0 License.

Wang, Q., Danilov, S., Sidorenko, D., Timmermann, R., Wekerle, C., Wang, X., Jung, T., and Schröter, J.: The Finite Element Sea Ice-Ocean Model (FESOM) v.1.4: formulation of an ocean general circulation model, Geoscientific Model Development, 7, 663–693, https://doi.org/10.5194/gmd-7-663-2014, publisher: Copernicus GmbH, 2014.

Wehrli, K., Guillod, B. P., Hauser, M., Leclair, M., and Seneviratne, S. I.: Assessing the Dynamic Versus Thermodynamic Origin of Climate Model Biases, Geophysical Research Letters, 45, 8471–8479, https://doi.org/10.1029/2018GL079220, _eprint: https://onlinelibrary.wiley.com/doi/pdf/10.1029/2018GL079220, 2018.

Wehrli, K., Hauser, M., and Seneviratne, S. I.: Storylines of the 2018 Northern Hemisphere heatwave at pre-industrial and higher global warming levels, Earth System Dynamics, 11, 855–873, https://doi.org/10.5194/esd-11-855-2020, publisher: Copernicus GmbH, 2020.

Zappa, G.: Regional Climate Impacts of Future Changes in the Mid–Latitude Atmospheric Circulation: a Storyline View, Current Climate Change Reports, 5, 358–371, https://doi.org/10.1007/s40641-019-00146-7, 2019.

Zhang, Y. and Boos, W. R.: An upper bound for extreme temperatures over midlatitude land, Proceedings of the National Academy of Sciences, 120, e2215278 120, https://doi.org/10.1073/pnas.2215278120, publisher: Proceedings of the National Academy of Sciences, 2023.

Zängl, G., Reinert, D., Rípodas, P., and Baldauf, M.: The ICON (ICOsahedral Non-hydrostatic) modelling framework of DWD and MPI-M: Description of the non-hydrostatic dynamical core, Quarterly Journal of the Royal Meteorological Society, 141, 563–579, https://doi.org/10.1002/qj.2378, _eprint: https://onlinelibrary.wiley.com/doi/pdf/10.1002/qj.2378, 2015.